Lithos 204 (2014) 4–13

Contents lists available at ScienceDirect

Lithos

journal homepage: www.elsevier.com/locate/lithos

Mantle origin of the Emeishan large igneous province (South China) from the analysis of residual gravity anomalies

Yangfan Deng [a,b,*], Zhongjie Zhang [b], Walter Mooney [c], José Badal [d], Weiming Fan [a], Qiu Zhong [e]

[a] Guangzhou Institute of Geochemistry, Chinese Academy of Sciences, Guangzhou 510640, China
[b] State Key Laboratory of Lithospheric Evolution, Institute of Geology and Geophysics, Chinese Academy of Sciences, Beijing 100029, China
[c] U.S. Geological Survey, 345 Middlefield Road, MS 977, Menlo Park, CA 94025, USA
[d] Physics of the Earth, University of Zaragoza, Pedro Cerbuna 12, 50009 Zaragoza, Spain
[e] University of Chinese Academy of Sciences, Beijing 100049, China

ARTICLE INFO

Article history:
Received 5 June 2013
Accepted 10 February 2014
Available online 20 February 2014

Keywords:
Stripping
Residual gravity anomaly
Density anomaly model
Mantle plume
Emeishan igneous province
South China

ABSTRACT

Despite numerous geologic and geochemical studies conducted on the Emeishan Large Igneous Province (LIP) in SW China, the deep origin of this LIP is still poorly constrained. Here we investigate the residual gravity anomaly in South China, and its relationship to the Emeishan LIP, in conjunction with deep seismic sounding profiles, deep seismic reflection surveys and a variety of broadband seismic observations performed in South China during the past few decades. Our analysis includes the removal of related gravitational effects due to: (1) the sediments, (2) the crystalline basement, undulations of (3) the upper crust, (4) the Moho and (5) the mantle lid. The resultant residual gravity anomaly in the Emeishan LIP and surrounding region reaches a maximum value of +150 mGal and decreases gradually with distance from this inner zone. With the conjugate gradient method, we develop a lithospheric model consisting of a cylindrical-shaped positive density anomaly that provides a good fit to the observed residual gravity anomaly. The inverted density anomaly of the Emeishan LIP is +0.06 g/cm^3 in the inner zone and decreases to about +0.03 g/cm^3 in the outer zone. The observed positive residual gravity and the corresponding high density can be attributed to mafic/ultramafic rocks and cooled surrounding rocks generated by large scale magmatic intrusion. Hence, taking account of the Permian Emeishan LIP, our residual gravity and density model provide evidence for the formation by an upwelling of a mantle plume.

1. Introduction

A mantle plume is the ascent of hot buoyant material toward the Earth's surface or the base of the lithosphere (Griffiths and Campbell, 1991; Larson, 1991; Leng and Zhong, 2010). As the top/head of a mantle plume can partially melt when it reaches shallow depths and pressure is reduced, they are thought to be the cause of volcanic centers and flood basalts (Campbell and Griffiths, 1990; Coffin and Eldholm, 1994; Morgan, 1971; White and McKenzie, 1989; Zhao, 2001). The plume hypothesis has been widely adopted to explain the formation of age-progressive volcanic chain hotspots such as Hawaii and Large Igneous Provinces (LIPs) in both oceanic and continental settings (Campbell and Griffiths, 1990; Coffin and Eldholm, 1994; Morgan, 1971; White and McKenzie, 1989; Xu et al., 2004, 2007; Zhao, 2001, 2007; Zhong and Watts, 2002).

The Late Permian basalts of the Emeishan LIP are erosional remnants of mafic rock from a series of voluminous volcanic eruptions that occurred in the western margin of the Yangtze Craton (Xu et al., 2004, 2007). Previous studies have documented that the main phase of the flood basalt volcanism occurred at the Middle-to-Late Permian boundary that is estimated at 260 Ma (Gradstein et al., 2012). The total age span of the Emeishan basalts has been estimated to be in the range of 251–263 Ma (Xu et al., 2007), but more recent chronological studies suggest that the Emeishan volcanics were emplaced during a very short period (<2 m.y.) at ~259 Ma (Shellnutt et al., 2012; Zhong et al., submitted for publication).

The Emeishan LIP lies within a rhombus-shaped area of 250,000 km^2 bounded by the Longmenshan fault to the northwest and the Red River fault to the southwest (Xu et al., 2001). In recent years, the Emeishan LIP has attracted the attention of the scientific community because of its possible synchrony with the eruption of the end-Permian mass extinction (Ali et al., 2002; Chung and Jahn, 1995; Chung et al., 1998; Lo et al., 2002; Shellnutt, 2013; Wignall et al., 2009; Wu and Zhang, 2012).

A recent review shows that there are seven convincing arguments in support of a Permian mantle plume origin for the Emeishan LIP, namely: (1) pre-volcanic crustal uplift, (2) high-temperature magmas, (3) thermal zoning structure, (4) geochemistry, (5) duration of volcanism, (6) extent and volume of volcanism, (7) physical volcanology (Xu et al., 2007). From the sedimentological and paleogeographic data, the

* Corresponding author at: State Key Laboratory of Lithospheric Evolution, Institute of Geology and Geophysics, Chinese Academy of Sciences, Beijing 100029, China.
E-mail address: dengyangfan@mail.iggcas.ac.cn (Y. Deng).

http://dx.doi.org/10.1016/j.lithos.2014.02.008
0024-4937/

dome-shaped structure associated with the Emeishan LIP can be divided into three zones, the inner, middle and outer zones, according to the extent of erosion of the Maokou Formation composed of Mid–Late Permian carbonates (He et al., 2003; Xu et al., 2004) (Fig. 1). The boundary between the inner and middle zones is the Xiaojiang fault to the east (labeled F7 in Fig. 1). The extent of erosion is the most apparent in the inner zone that is proposed to be the site of a rising plume head (He et al., 2003).

Many geological and geochemical studies have been conducted on the Emeishan LIP, but the deep origin is still poorly constrained. Globally, there has been an increasing body of evidence for the existence of deep mantle plumes, particularly on the basis of the results supplied by seismic tomography (Goes et al., 1999; Lei and Zhao, 2006; Lü et al., 2013; Montelli et al., 2004, 2006; Rhodes and Davies, 2001; Ritsema and Allen, 2003; Romanowicz and Gung, 2002; Zhao, 2001). In this paper we assess the mantle plume model for the Emeishan LIP based on a detailed modeling of gravity data, because neither the seismic P-wave nor S-wave velocities by themselves provide sufficient information about the density structure of the lithosphere (Mooney and Kaban, 2010). The cratonic roots, which show positive S-wave velocities, offer a clear example of the ambiguity of the seismic models for determining lithospheric density. These cratonic roots present near-zero density anomalies because their low temperatures (which increase density) are compensated by the low Fe composition of the root. Thus, gravity data provide valuable constraints on the physical state of the lithosphere that are complementary to the seismic data, and may shed more light on geodynamic processes in the region. For example, density variations in the lithosphere and sublithospheric mantle play an important role in controlling the surface elevation.

Measured Bouguer gravity is a summation of all density anomalies within the lithosphere including the density difference to the reference model within the layers and the undulation of intra-crustal and sub-crustal layers (Fig. 2) (Q.S. Wang et al., 2003; Zeng, 2005). In this paper we investigate the residual gravity of the Emeishan LIP through a process of gravity-stripping that consists of the systematic calculation of 3D corrections to the observed Bouguer gravity. We obtain the residual gravity by removing the effects caused by the sediments, crystalline basement and the undulation of the lithospheric layers as inferred from deep seismic sounding profiles, deep seismic reflection surveys, and a variety of broadband seismic observations (Bai et al., 2011; Deng et al., 2011; Hu et al., 2003; Li et al., 2006; C.Y. Wang et al., 2003; Xiong et al., 2009; Zhang et al., 2009, 2010). The consequent residual gravity mainly reflects the compositional density anomaly (the circles in Fig. 2) of the lithosphere beneath the study area, which in turn is correlated with the geological evolution of the Emeishan LIP.

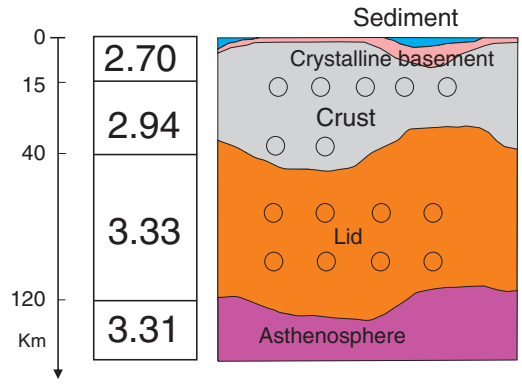

Fig. 2. Left: the reference lithospheric/asthenospheric structure described in terms of the respective depths and densities (in g/cm^3) of the major layers. Right: sketch illustrating the laterally varying lithosphere in South China. The circles indicate the compositional density anomaly of the lithosphere to the reference model within the layers.

2. Data processing and gravitational effects

In order to better understand the gravity anomaly of the Emeishan LIP, we first analyze the data on a larger scale. Pavlis et al. (2008, 2012), who presented the Earth Gravitational Model (EGM2008), computed the original Bouguer gravity over South China and surrounding region. This model has a grid spacing of 2.5 × 2.5 arc-minute in both land and ocean. The standard deviation of the Bouguer gravity data in this area is less than 5 mGal (Pavlis et al., 2008). As shown in Fig. 3, in South China, small positive gravity anomalies (< + 100 mGal) are confined to regions near the ocean and offshore. Considering a larger geographic area, negative gravity anomalies (about − 200 mGal) can be

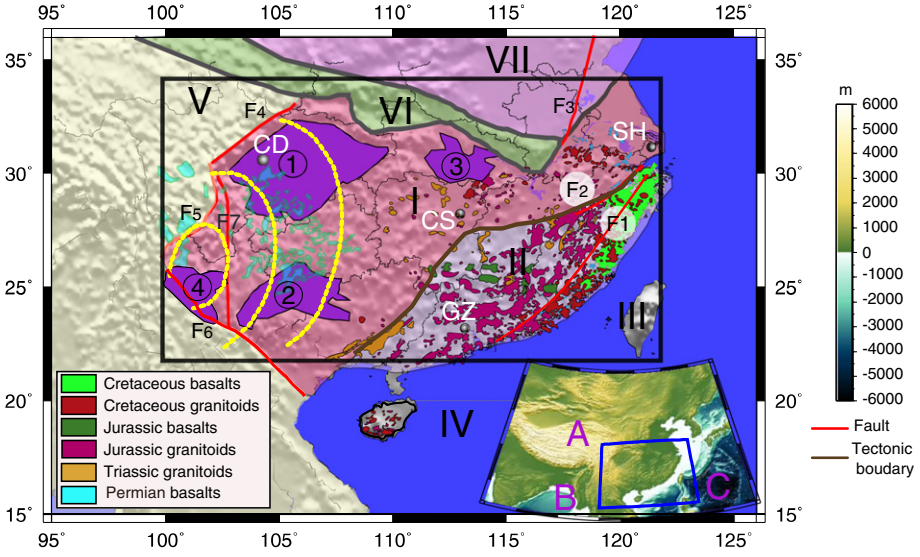

Fig. 1. Topographic relief and tectonic units in South China (location map is in the bottom right corner). The central rectangle drawn by black lines depicts the study area. The yellow dashed lines indicate the inner, middle and outer zones of the Emeishan Large Igneous Province (LIP). The spatial distribution of the Mesozoic magmatic rocks is based on Chen et al. (2008) and Liu et al. (2012); the distribution of the Permian basalts is based on Xu et al. (2004, 2007). A: Asian plate; B: Indian plate; C: Philippine Sea plate; I: Yangtze Block; II: Cathaysia Block; III: Taiwan orogen; IV: South China Sea basin; V: East of Songpan–Ganzi Block; VI: Qinling–Dabie orogen; VII: North China Block; F1: Zhenghe–Dapu fault belt; F2: Jiangshan–Shaoxing fault belt; F3: Tanlu fault belt; F4: Longmenshan fault belt; F5: Anninghe fault belt; F6: Red River fault belt; F7: Xiaojiang fault belt; CD: Chengdu city; CS: Changsha city; SH: Shanghai city; GZ: Guangzhou city. There are four main basins in South China, namely: ① Sichuan basin; ② Jianghan basin; ③ Nanpanjiang basin; ④ Chuxiong basin.

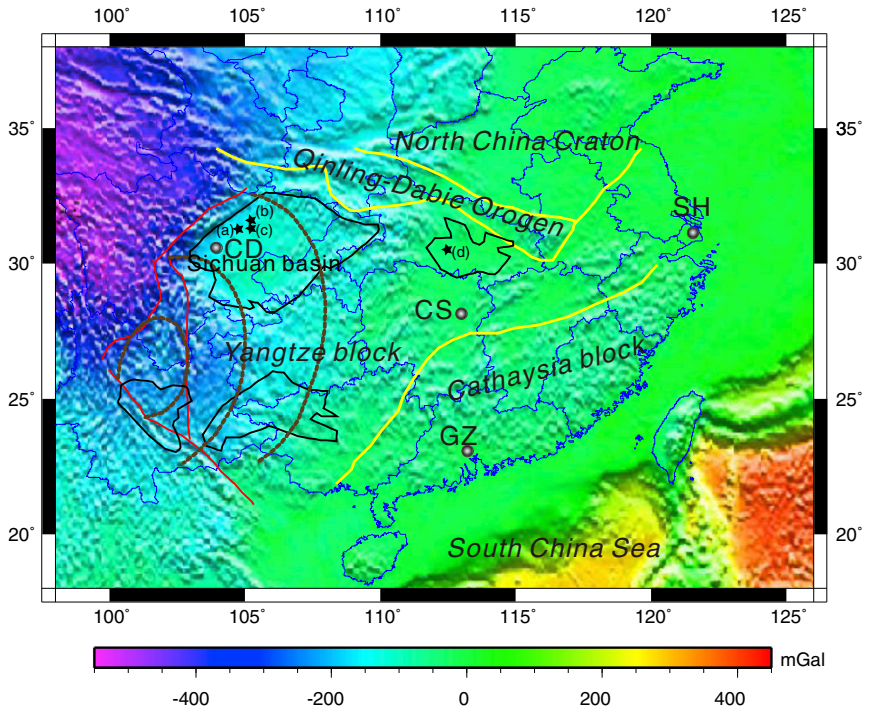

Fig. 3. Bouguer gravity map of South China and surrounding regions (after Pavlis et al., 2008, 2012). The tectonic units are the same as in Fig. 1. The circular lines on the left half of the plot outline the inner, middle and outer zones of the Emeishan LIP. The four stars (a), (b), (c) and (d) correspond to the locations of four wells discussed in Fig. 4. Small positive gravity anomalies (<+100 mGal) are confined to regions near the oceanic areas. At a larger scale, small negative gravity anomalies (about −200 mGal) can be observed in part of the Qinling–Dabie orogen, Sichuan basin and the rhombus shaped area. Within the Songpan–Ganzi block, the Bouguer gravity progressively decreases in a westward direction to more negative values, to reach up to −550 mGal.

observed in parts of the Qinling–Dabie orogen and the Sichuan basin. In the Songpan–Ganzi block of the Tibetan Plateau, the Bouguer gravity decreases westward to progressively more negative values, reaching up to −550 mGal. Thus, this pattern can be summarized as follows: the higher the elevation of the ground, the greater the negative Bouguer gravity anomaly (Deng et al., 2013). However, it is hard to find the correlation between the gravity anomaly and the circular regions representing the inner, middle and outer zones of Emeishan LIP (Fig. 3). Therefore, although the topography and free-air effects have been removed from the Bouguer gravity, in order to isolate the gravity response of Emeishan LIP we have to remove other gravitational effects, in particular those caused by the sedimentary cover, crystalline basement, the undulation of the upper crust, Moho and the lithosphere. This sequential procedure, referred to as *stripping*, was first described by Hammer (1963) and later developed by other authors (Bielik, 1988; Bielik et al., 2013a, b; Mooney and Kaban, 2010).

Low-density sediments result in a negative gravity anomaly relative to the crystalline crust. Thus removing this sedimentary effect will increase the residual anomaly. We must also account for depth variations of the crystalline basement. An uplift of the Moho discontinuity produces a positive gravity anomaly and leads to a reduction in the residual anomaly. In contrast, a depression of the Moho produces a negative anomaly; the same is true for undulations of the lithosphere, which is here assumed to be 0.02 g/cm^3 denser than the underlying asthenosphere.

It is generally assumed that any change affecting the horizontality of the homogeneous reference density model would lead to a change in the residual gravity anomaly (Mooney and Kaban, 2010), whereas the gravity from a uniform horizontal layer with invariable density is a constant. Our reference model (Fig. 2) corresponds to a continental crust with flat topography, and consisting of a 15-km-thick upper crust with a density of 2.7 g/cm^3 (Mooney and Kaban, 2010), and a 25-km-thick lower crust with a density of 2.94 g/cm^3 (Deng et al., 2011; Mooney and Kaban, 2010). The average density of the mantle lithosphere is set equal to 3.33 g/cm^3, while that of the asthenosphere is 3.31 g/cm^3 (Burov, 2010).

Forward modeling of gravity data is a linear problem (Li and Oldenburg, 1998; Nagy, 1966). The vertical component of the gravity field at a point (x, y, z) produced by the density ρ(x, y, z) is given by

$$F\left(\vec{r_0}\right) = G\int_V \rho\left(\vec{r}\,\frac{z-z_0}{|\vec{r}-\vec{r_0}|^3}\right)dv$$

where $\vec{r_0}$ (x_0, y_0, z_0) is the vector defining the observation point and $\vec{r}$ (x, y, z) denotes the position vector of the point source mass. V represents the volume of the anomalous mass, and G is the gravitational constant. To implement the procedure we divide the volume of interest into a set of 3D prismatic cells, which have azimuth (i, j) and height k, by using a 3D orthogonal mesh and assume a constant density within each cell. The gravity at surface can be obtained through the equation

$$F(x_0, y_0) = G\sum_{i,j,k}\rho_{i,j,k}\frac{V_{i,j,k}\left((x_i-x_0)^2+(y_j-y_0)^2+z^2\right)\Big)^{1/2}}{\left((x_i-x_0)^2+(y_j-y_0)^2+z^2\right)^{3/2}}$$

where $V_{i,j,k}$ is the volume of each cell.

2.1. Gravitational effect of the sediments

The first step in processing the Bouguer gravity field consists of removing the effect of the sedimentary cover. To this end we need know the geometry (elevation and thickness) and density for each grid cell in which the medium has been subdivided. A significant amount of data is available on the sedimentary basins in South China (Li and Li, 2007; Wang, 2009; Wang et al., 2006) and these investigations are useful to constrain the features of the basin. The density measurements in three boreholes located in the central and western parts of Sichuan

basin (Liu and Chang, 2003) and one borehole located in the Jianghan basin (Wang et al., 2010) are shown in Fig. 4. The densities determined in these four boreholes range between 2.4 g/cm^3 and 2.6 g/cm^3, and the average density of the sedimentary materials is assumed to be 2.5 g/cm^3.

We have compiled a set of thickness data for the sediments within the basins with the aid of national institutions such as the Chinese National Petroleum Company, the Chinese National Oil and Natural Gas Company and the China Ocean Petroleum Company (Li and Zhou, 1990; Luo and Tong, 1988; Zhang et al., 1996). The dashed black lines in Fig. 5 (upper plot) outline the region where we collected sedimentary thickness data from the review by Z. Zhang et al. (2011), while in other regions the sediment thickness data were taken from the global digital model of Laske and Masters (1997). Fig. 5 (upper plot) shows the map of the sediment thickness in South China, which varies considerably from one location to another. For example, the Sichuan basin locally has the largest sediment thickness, about 9 km, while the Jianghan and Nanpanjiang basins have a maximum sediment thickness of about 4 and 2 km, respectively.

Next, we constructed the 3D density model for the sediments and calculated its gravitational effect. This is a linear problem that involves determining the vertical component of the gravity field caused by an anomalous excess or defect of mass below surface (Li and Oldenburg, 1996, 1998). Fig. 5 (lower plot) shows the gravitational effect in this case. The largest anomaly caused by the sediments is −80 mGal and is located in the Sichuan basin.

2.2. Gravitational effect of the crystalline basement

Following the gravity-stripping process as applied through the prismatic cell model, we removed the effect of the undulated crystalline basement, which is defined by the depth of the seismic velocity contour of 6.0 km/s as measured from deep seismic sounding profiles (Nielsen and Thybo, 2009). The spatial variation of the crystalline basement was obtained from the data provided by 57 seismic profiles performed in South China (Deng et al., 2011) and using kriging interpolation, which is a robust estimator that permits us to model both regional trends and local anomalies (Davis, 1986; Serón et al., 2001). The density of the crystalline basement was assumed to be 2.67 g/cm^3 (Wang et al., 1997). Fig. 6 (upper plot) shows the crystalline basement thickness in South China, with the smaller values distributed over the Emeishan LIP. As before, we computed the gravitational effect caused by the undulations of the crystalline basement and the corresponding anomalous excess or deficit of mass. Fig. 6 (lower plot) shows the corresponding gravitational effect on a map of the region. The gravity anomaly is small everywhere, having a value close to zero in the Sichuan basin. The largest value, about −30 mGal, is found to the west of the study area.

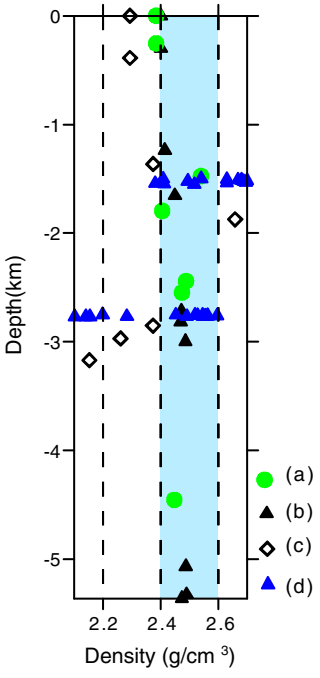

Fig. 4. Density measurements in three boreholes located in Sichuan Basin (Liu and Chang, 2003) and one borehole located in the Jianghan Basin (Wang et al., 2010): (a) Chunxiao 93 well; (b) Chuanfeng 131 well; (c) Chuanhe 100 well log data; (d) Jianghan Wb10-7 well. The measured density was found to be between 2.4 g/cm^3 and 2.6 g/cm^3, so the density of the sedimentary materials was set to 2.5 g/cm^3.

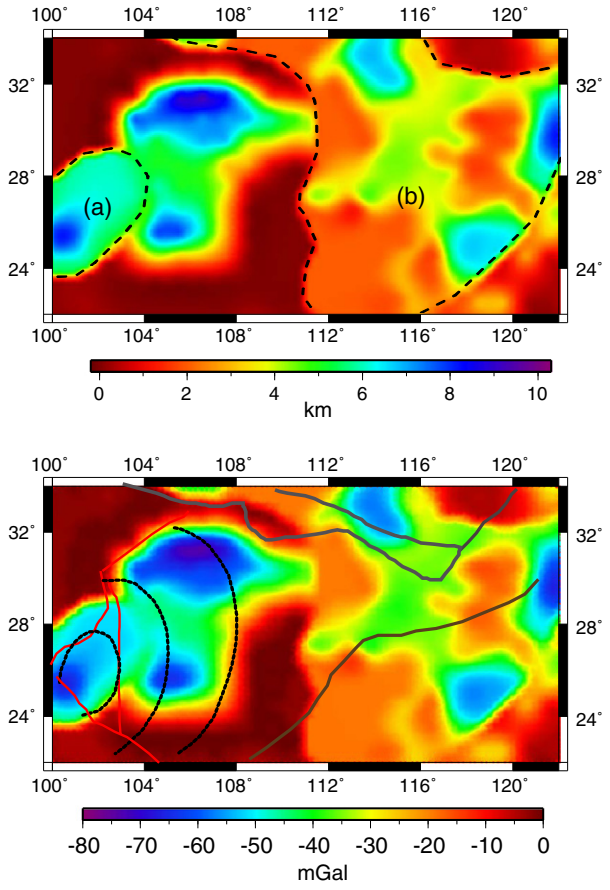

Fig. 5. Upper panel: sediment thickness in South China and surrounding regions. The dashed black lines (a) and (b) enclose the thickness data we collected, while the thickness data in other areas were extracted from a global digital map (Laske and Masters, 1997). Sichuan basin has the greatest sediment thickness, about 9 km, whereas the Jianghan and Nanpanjiang basins have a sediment thickness of about 4 and 2 km, respectively, although in most of the study area the thickness hardly reaches 1 km. Lower panel: gravitational effect of the undulated sediment cover. The tectonic units outlined by solid lines are the same as in Fig. 1. The circular lines on the left half of the plot outline the inner, middle and outer zones of Emeishan LIP. The biggest negative gravity anomaly caused by the sediments is of about −80 mGal and is located in Sichuan basin.

2.3. Gravitational effect of upper crustal thickness variations and Moho undulations

Thousands of experiments using a variety of seismic techniques have confirmed the existence of a well-defined crust/mantle discontinuity (Moho) on global scale, and furthermore, that the Moho depth varies systematically beneath different tectonic blocks, depending on their age and the particular tectonic environment (Christensen and

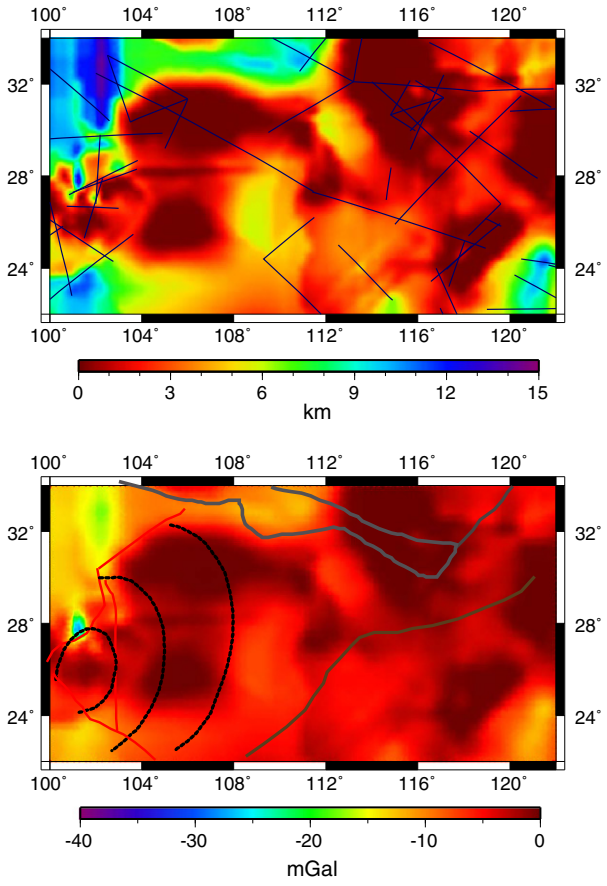

Fig. 6. Upper panel: mapping of the crystalline basement thickness in South China and surrounding regions. The straight lines represent positions of deep seismic soundings; more details can be found in Deng et al. (2011). The sediment thickness is less than 3 km in the majority of the explored area. Lower panel: gravitational effect of the undulated crystalline basement. The tectonic units outlined by solid lines are the same as in Fig. 1. The circular lines on the left half of the plot outline the inner, middle and outer zones of Emeishan LIP. The negative gravity anomaly is small everywhere and close to zero in Sichuan basin, and its largest value of about −40 mGal is found in west of the study area.

Mooney, 1995; Mooney et al., 1998; Prodehl and Mooney, 2012). Several seismological methods are commonly used to probe this discontinuity between crust and mantle, including refraction/wide-angle reflection surveys (Li et al., 2006; Teng et al., 2013; Z. Zhang et al., 2011; Z.J. Zhang et al., 2011), near-vertical seismic reflection profiling (Braile and Chiang, 1986; Mooney and Meissner, 1992), and P/S wave receiver functions (Chen et al., 2006; Tian et al., 2011). Of these methods controlled-source refraction/wide-angle reflection surveys are the most accurate (Teng et al., 2013). Numerous deep seismic profiles have been carried out in South China, with a total length over 20,000 km (Deng et al., 2011; Li et al., 2006; Z. Zhang et al., 2011; Z.J. Zhang et al., 2011). They provide the best resolution of the deep crustal seismic velocity structure. In our case the Moho depth was resolved from 57 deep seismic profiles carried out since 1970 (Deng et al., 2011). In those areas where the information is not constrained by seismic profiles, we refer to the Crust 2.0 model (Bassin et al., 2000). Due to the diverse geological features that make up South China, as such sedimentary basins, orogenic belts, and ultra-high pressure metamorphic rocks (Bai et al., 2007; Ratschbacher et al., 2000), the Moho depth varies greatly, reaching values of about 60 km to the west and 30 km to the east.

As to the crust as a whole, it is assumed that it may be divided into an upper crust and a lower crust. The former has a felsic bulk composition that is similar to granite (Wedepohl, 1995); however, the latter has an intermediate-to-mafic composition (Christensen and Mooney, 1995). Because of this difference in composition, there is a sharp density contrast for the upper and lower crustal layers. Therefore, the undulations of the boundary between the upper and lower crust should also be taken into consideration. Although we cannot accurately assess the thickness of the upper crust at all locations, measurements provided by seismic deep profiles in South China (C. Wang et al., 2003; Xiong et al., 1993; Zhu et al., 2005), indicate that the thickness of the upper crust amounts to half the total crustal thickness.

Undulations due to variations in total crustal thickness are significant. Fig. 7 (upper plot) shows the Moho depth in South China with values decreasing toward the ocean. Fig. 7 (lower plot) shows the gravitational effect due to undulations of the Moho. The negative gravity anomaly exceeds −100 mGal in the inner and middle zones of Emeishan LIP, corresponding to the deeper Moho, while the positive anomaly is about +160 mGal in the oceanic region.

2.4. Gravitational effect of the undulated mantle lithosphere

The undulations in the thickness of the sub-crustal lithosphere also exert an influence on the measured gravity anomaly. The lithosphere is defined as the cold and rigid outer shell of the Earth through which heat is transmitted by conduction. High-resolution seismic tomography

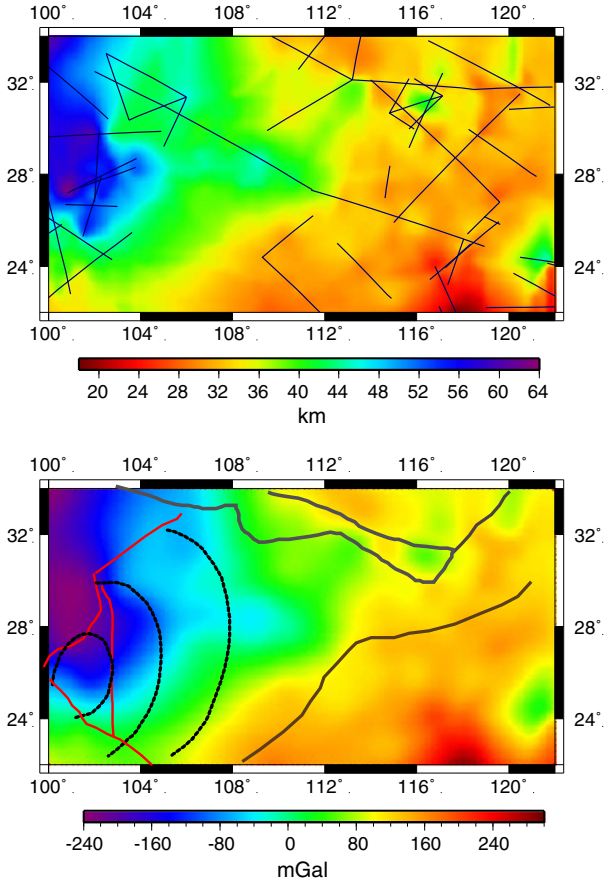

Fig. 7. Upper panel: crustal thickness in South China and surrounding regions. The straight lines represent positions of deep seismic profiles; more details can found in Deng et al. (2011). The crustal thickness varies gradually from west to east and the larger values occur in the western half of the study region. Lower panel: gravitational effect of the undulated crystalline crust. The tectonic units outlined by solid lines are the same as in Fig. 1. The circular lines on the left half of the plot outline the inner, middle and outer zones of Emeishan LIP. The negative gravity anomaly reaches −100 mGal in the inner and central sectors of Emeishan in correspondence with the deeper Moho, while the positive gravity anomaly is about +160 mGal and reaches +280 mGal in the oceanic regions.

velocity models have been commonly used in defining the lithosphere. The crust and the high-velocity layer of the uppermost mantle (the mantle lid) above the seismic low velocity zone (LVZ) are regarded as the seismic lithosphere. Zhu et al. (2006) estimated the lithosphere thickness in the entire China from seismic tomography. Because the boundary between the 'lid' and the LVZ, that is, the low velocity channel of the asthenosphere (Fig. 2), is not a sharp discontinuity, the different definitions of this 'boundary' can cause variations of several tens of kilometers in the estimated lithospheric thickness. Another important question is whether the seismic lithosphere estimated from seismic data, which have a time period measured in seconds is equivalent to the geodynamical lithosphere, which is considered for time periods many orders of magnitude longer.

Goes et al. (2000) developed a method to estimate the upper mantle temperature by inverting seismic velocities for temperature. Their work is based on laboratory measurements of density and elastic moduli for a variety of mantle minerals at high temperatures and pressures. This method, which is distinct from but complements geothermal modeling of heat flow data, provides a means to estimate the 3D upper-mantle temperature structure from measured seismic velocities. This temperature estimation method has been successfully applied in the studies of several continents (Cammarano et al., 2003; Goes and Van der Lee, 2002; Goes et al., 2000; Rohm et al., 2000; Shapiro and Ritzwoller, 2004). An and Shi (2006) calculated the 3D upper-mantle temperature structure of the Chinese continent from seismic velocities measurements in 3D, and used these results to estimate the lithospheric thickness on a $1^\circ \times 1^\circ$ grid, as shown in Fig. 8 (upper plot). The Yangtze craton has the greatest lithospheric thickness with a value about 180 km and more, whereas the Cathaysia block has a thickness of about 90 km. Fig. 8 (lower plot) shows the gravitational effect of the undulations of the deep lithosphere. A positive gravity anomaly, amounting to over +36 mGal, appears mostly distributed in the northwest quadrant of the study area as a consequence of the comparatively greater thickness of the lithosphere. The anomaly becomes −20 mGal in the southeast part where the lithosphere is thinner.

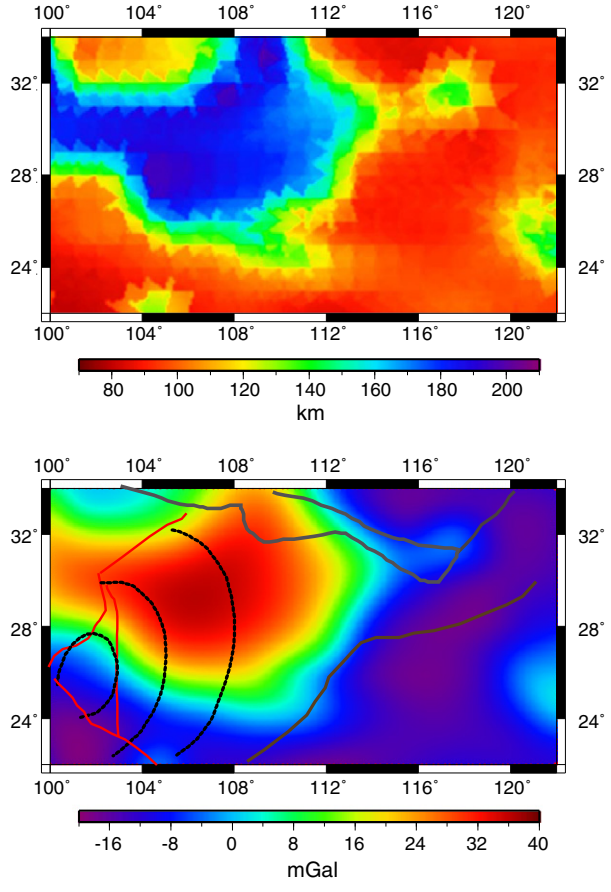

Fig. 8. Upper panel: mapping of the lithosphere thickness in South China and surrounding regions (An and Shi, 2006). Lower panel: gravitational effect of the undulated lithosphere. The tectonic units outlined by solid lines are the same as in Fig. 1. The circular lines on the left half of the plot outline the inner, middle and outer zones of Emeishan LIP. A positive gravity anomaly of about +36 mGal appears mostly distributed in the northwest quadrant of the study area as consequence of the comparatively greater thickness of the subcrustal lithosphere; however, the anomaly becomes −20 mGal in the southeast part where the lithosphere thickness is thinner.

3. Appraisal of model uncertainties

It is important to estimate the errors involved in the calculation of the residual gravity anomaly. Some important aspects of such an error analysis have been addressed by Panasyuk and Hager (2000) and Kaban and Schwintzer (2001). The overall error derives from uncertainties in: (1) the measured gravity and (2) the estimated thickness and density of (a) the sediment; (b) the crystalline basement; (c) the upper crust; (d) the lower crust; and (e) the mantle lid. Of all these factors, the error associated with the observed satellite gravity is the smallest one, as it amounts to only 5 mGal (Pavlis et al., 2008, 2012). However, the other factors may give rise to larger errors, with a magnitude of 10 mGal or more.

In our modeling we consider the density in the sediment, crystalline basement, upper crust, lower crust and sub-crustal lithosphere to be a constant, which is a simplification of the real conditions considering the data supplied by the boreholes described in Section 2.1 (Fig. 4) and the standard deviation of the average global crustal density structure (Christensen and Mooney, 1995). The uncertainty in density is estimated to be 0.1, 0.03, 0.1, 0.04 and 0.02 g/cm^3, respectively. The sediment thickness in our study can be estimated with an error around 1 km at a scale of $1^\circ \times 1^\circ$ (Laske and Masters, 1997), and the resultant error calculated for the gravity anomaly would be of about 10 mGal. The depth of the crystalline basement can be estimated with an error of some 3 km, which leads to an induced error in gravity of the order of 10 mGal.

Seismic refraction/wide-angle reflection data provide the most reliable measurements of crustal seismic structure, and the measurement error depends on the data quality and coverage. For example, if we rely on seismic profiles recorded before the 1990s, the uncertainty in the Moho depth could be up to 10% (4–5 km) (Mooney and Kaban, 2010; Mooney et al., 1998). However, when we consider a region sufficiently explored by more recent seismic profiles, the uncertainty can be reduced to 5% (2 km). In those areas lacking seismic soundings or with less coverage, the uncertainty could be of 3–5 km or more. These depth uncertainties correspond to an error between 30 and 60 mGal. As described in Section 2.3, the crust structure in some profiles in South China can be equally divided into an upper crust and a lower crust. However, there is an uncertainty in the thickness of the upper crust in the regions where the crust structure may consist of three layers. Likewise there is a large uncertainty (~5 km) for the region lacking seismic profile coverage (Jia et al., 2006; Yao et al., 2007). In such cases the uncertainty in the gravity anomaly is 50 mGal.

Lastly, the uncertainty in the estimation of the thickness of the lithosphere is about 10% (An and Shi, 2006), which corresponds to an uncertainty in depth of 20 km and error in gravity less than 5 mGal. All these uncertainties are summarized in Table 1.

It should be noted that the relative weight of these factors depends on the available data coverage, and, furthermore, since these uncertainties are not correlated, the total uncertainty is usually less than the total sum of them (Mooney and Kaban, 2010). For example, the areas with a thick crust are generally characterized by a thin sedimentary cover and a well-defined Moho. By combining all error sources, the cumulated error inherent to the gravity anomaly varies between 195 mGal for the well-studied regions of South China with thin consolidated crust,

Table 1
Estimated uncertainties related to layer thickness, density and induced gravity anomaly.

Source	Uncertainty in thickness (km)	Uncertainty in density (g/cm^3)	Uncertainty in anomaly (mGal)
Observed gravity			Less than 5
Sedimentary cover	1	0.10	About 35
Crystalline basement	3	0.03	Less than 15
Upper crust	5	0.10	About 70
Undulation of the Moho	3–5	0.04	50–80
Mantle lithosphere	20	0.02	About 20

and 225 mGal for the regions with thick crust and poor seismic coverage. As we shall see in the next section, the residual gravity anomaly ranges from −280 to +240 mGal, yielding a signal-to-noise ratio significantly higher than 1.

4. Residual gravity anomaly and 3D density model

The progressive step-by-step elimination of the gravitational effects associated with the sediments, the crust and mantle lithosphere, allows us to obtain the residual gravity anomaly in the Emeishan LIP as illustrated in Fig. 9. From the stripped, residual gravity map in Fig. 9d we find a remarkable positive anomaly (up to +100 mGal) extending on the inner, middle and outer zones of the igneous province, which in turn decreases gradually and becomes a negative anomaly beyond the Emeishan LIP. The residual gravity displayed in Fig. 9d has a close relationship with the spatial distribution of the Emeishan igneous province, even though not all regions with volcanic rocks in the Emeishan LIP show a positive anomaly. Taking account of the fact of the Permian Emeishan LIP, we interpret this correlation as evidence of the cooled remnants of the Late Permian mantle plume that generated this igneous province. In particular, the inner zone presents a relatively higher value anomaly (up to +150 mGal) than the middle zone and the outer zone, which is consistent with the spatially varying thickness of the Maokou Formation (He et al., 2003), and also is in good agreement with the petrologic evidence that the melt production was higher in the inner zone than in other zones (Xu et al., 2004, 2007).

Although the origin of the Emeishan LIP has long been debated, the mantle plume model is strongly supported by petrologic and geochemical evidence, and particularly the presence of high temperature basalts in the area (Chung and Jahn, 1995; Xu et al., 2001, 2007; Zhang et al., 2006). The magma must have intruded through the whole lithosphere since the basalts have a sub-lithospheric mantle origin, and in some cases would become contaminated by lithospheric material, thus altering its composition (Wu and Zhang, 2012), and showing coupled features from the PmS and SKS splitting (Chen et al., 2013; Sun et al., 2013).

In order to locate and interpret the deep origin of the residual gravity source, we inverted the available gravity data by using the conjugate gradient method. We first constructed a rectangular mesh with dimensions 0.25° × 0.25° × 500 m to produce cuboids as the initial density model. The initial density structure is based on the constraints from geophysical surveys and geological data (e.g. measurements of high seismic velocities in the mantle lithosphere, lower crust and upper crust, and the basalts exposed at the surface) (Liu et al., 2001; Xu et al., 2007). We then adjusted the densities within the cuboids, calculate the resultant gravity anomaly, and iteratively fit the observed residual anomaly. Fig. 10a

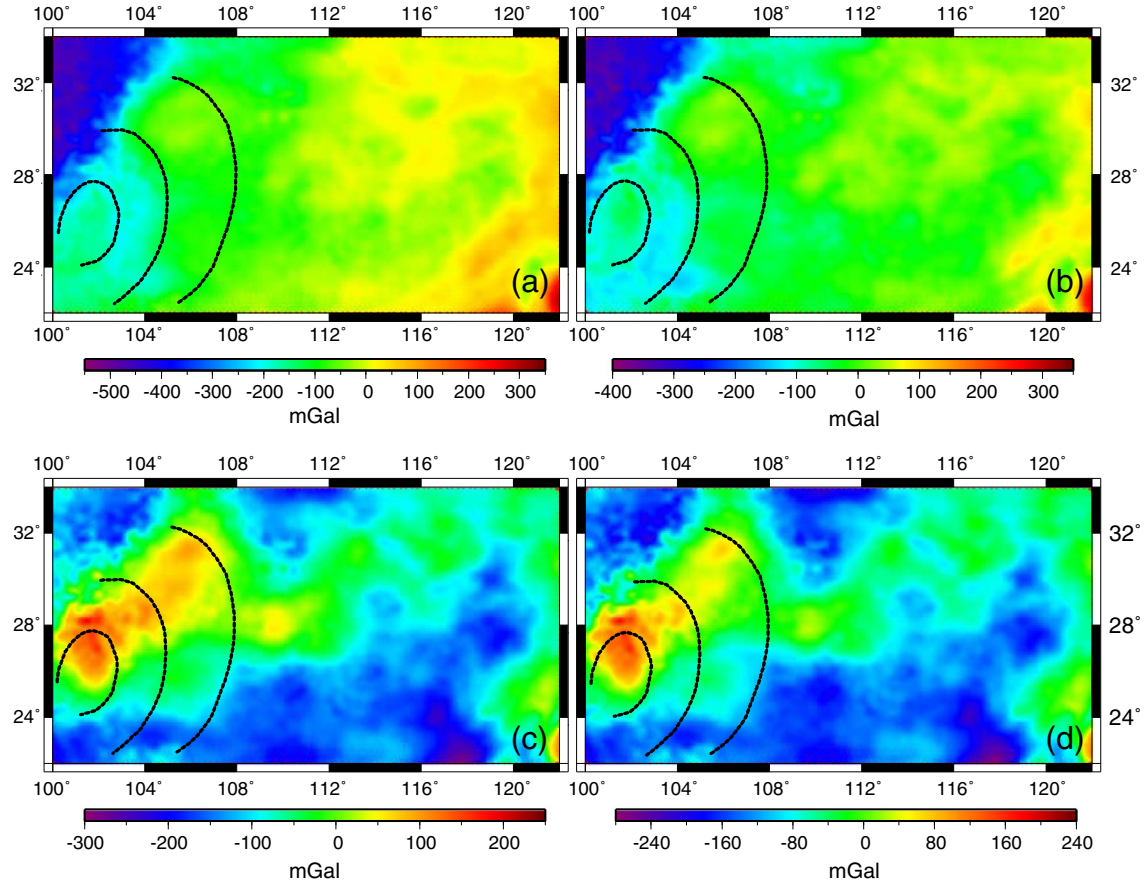

Fig. 9. Stripped residual gravity anomaly in South China after removing successively from the Bouguer gravity the gravitational effects associated to the sediments, the crust and upper mantle: (a) Bouguer gravity − $G_{sediment}$; (b) Bouguer gravity − $G_{sediment}$ − $G_{crystalline\ basement}$; (c) Bouguer gravity − $G_{sediment}$ − $G_{crystalline\ basement}$ − G_{upper_lower} − G_{crust}; (d) Bouguer gravity − $G_{sediment}$ − $G_{crystalline\ basement}$ − G_{upper_lower} − G_{crust} − $G_{lithosphere}$. In each case G makes reference to the gravitational effect due to the structure indicated by the subscript. The subscript upper_lower refers to the undulated layer between the upper and lower crust. The circular lines on the left half of the plot outline the inner, middle and outer zones of Emeishan LIP. A remarkable positive anomaly (up to +150 mGal) spreads over the inner, central and outer zones of the igneous province (plot (d) in the bottom right quadrant).

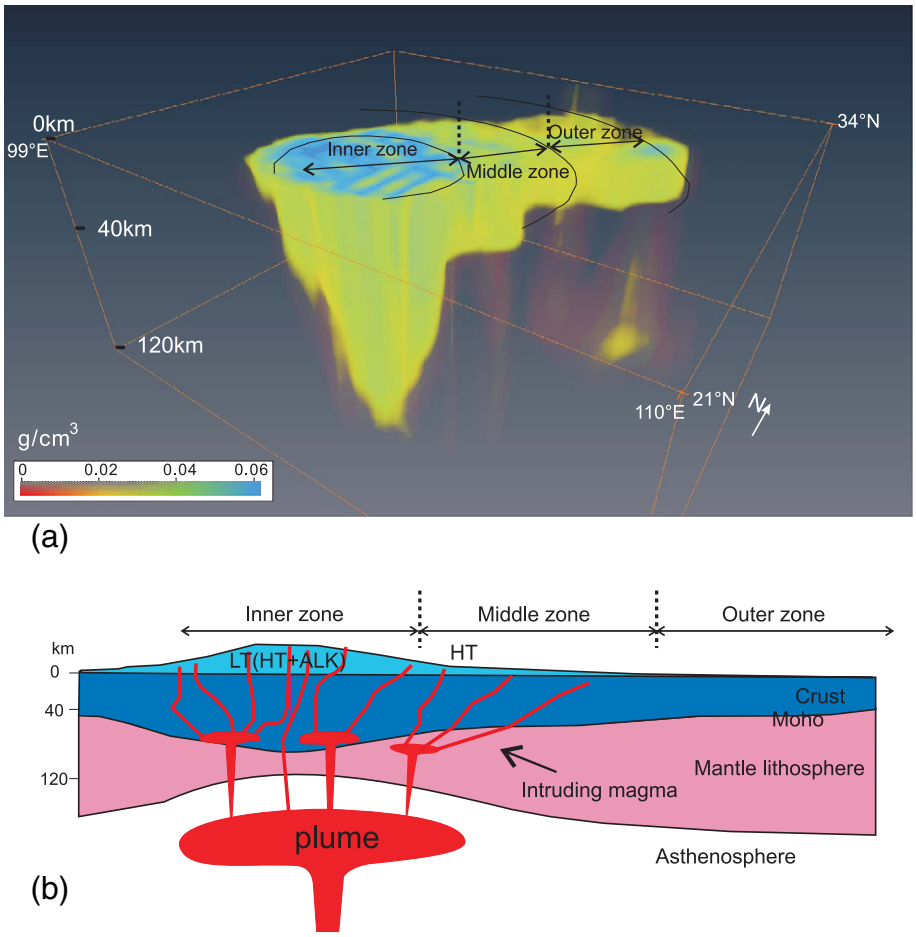

Fig. 10. (a): 3D density anomaly model based on the residual gravity anomaly measured in Emeishan LIP. The density anomaly decreases from +0.06 g/cm^3 to +0.03 g/cm^3 from the inner zone to outer zone (delimited by circular lines drawn on surface). (b): Schematic diagram illustrating the origin of the Emeishan basalts as the result of hot upwelling mantle material, the intrusion of melt into the crust and lithosphere, and the elevation of the ground surface, all by action of a mantle plume (modified from Shellnutt, 2013; Xu et al., 2004). LT: low-Ti basalt; HT: high-Ti basalt; ALK: alkaline series.

shows the final density model that extends to a depth of 120 km. This model provides an excellent fit (±10 mGal) to the residual gravity anomaly. The inner zone has a higher density anomaly (+0.06 g/cm^3) than the middle (+0.04 g/cm^3) and outer (+0.03 g/cm^3) zones. In other words, the affected volume expands as it approaches the surface, while its influence decreases radially away from the inner zone.

A mantle plume model has been illustrated by using literature geophysical and geochemical data (Xu and He, 2007; Xu et al., 2004). The lithospheric density anomaly model presented here (Fig. 10a) not only fits our observed residual gravity, but also agrees with what would be expected for a plume model (Fig. 10b). The predominance of the thick low-Ti intrusions in the inner zone suggests that the mantle beneath the core of the domal structure underwent more extensive partial melting as a result of a higher temperature than did the mantle beneath the marginal area. This inference and the occurrence of picrites in the inner zone, are consistent with a hotter mantle beneath the center of the dome than beneath the dome periphery (Xu et al., 2004). We envision the following scenario. As the Late Permian plume head invaded the lithosphere mainly in the inner zone, the magma intruded divergently into the mantle lithosphere and crust along existing faults. Abundant basalts and ultramafic melt with high temperatures intruded the crustal rocks and the density of the rock mass gradually increased with time. These remnants of intruded rock and cooled surrounding rock could account for the present positive residual gravity and density anomaly. The inner zone was affected to a greater degree by the mantle plume than the other zones, as indicated by: (1) sedimentologic evidence for kilometer-scale, pre-volcanic uplift and/or doming, including thinning of marine carbonates, a marine to subaerial transition, a local provenance of clastic sediments, and a marked erosional unconformity, evident like paleo-karstic surfaces on the marine carbonates (He et al., 2003, 2006; Xu et al., 2004); (2) variations in the flood-basalt geochemistry (Low-Ti basalt, High-Ti basalt and alkaline series rocks) from the center to the edge of the dome-shaped structure (such that picrites are restricted to the core of the dome) that are interpreted as high-temperature melts in the center and lower temperature melts at the edge (Xu et al., 2004); (3) the crustal thickness, which ranges from 43 to 55 km in the inner zone, but is thinner (about 40 km) in the middle and outer zones (Deng et al., 2011; Liu et al., 2001; Xu and He, 2007); (4) variations in the thickness of volcanic rocks across the dome-shaped structure (Xu et al., 2004); (5) the spatial variation in residual gravity and the density anomaly as obtained in this study.

5. Conclusions

We have calculated and modeled the residual gravity anomaly associated with the Emeishan LIP. The method applied follows a gravity stripping process consisting of the progressive removal of the gravitational effect due to the sediments, the crystalline basement, the undulated crust and mantle lithosphere. The resultant residual gravity reaches +100 mGal in the Emeishan LIP, and the extent of the anomaly is larger (up to +150 mGal) within the inner zone and then decreases in the middle and outer zones. There is a consistent correlation between the mapped residual gravity and the extent of basaltic volcanic rocks mapped in the area.

We present a lithospheric density model to explain the residual gravity in South China, and propose that this gravity anomaly is associated with the late Permian Emeishan LIP. The inner zone has a higher density anomaly (+0.06 g/cm3) than the middle (+0.04 g/cm^3) and outer (+0.03 g/cm^3) zones. The remnants of mafic/ultramafic rocks and the cooled surrounding rock can account for the spatial variation in density anomaly and residual gravity. This, along with the seismic data and geochemical data, provides further support to the hypothesis that a Late Permian mantle plume gave rise to the Emeishan LIP.

Acknowledgments

The suggestions made by Xiaobo Tian, Yun Chen and Elizabeth Barnett, and the constructive comments made by Prof. Yigang Xu and two anonymous reviewers helped to greatly improve the manuscript. This work was sponsored by the National Basic Research Program of China (973 Program, grant 2011CB808904) and the National Nature Science Foundation of China (41021063). The support of the Earthquake Hazard Program of the US Geological Survey is gratefully acknowledged. The present work takes advantage of the Collaboration Agreement between the Institute of Geology and Geophysics, the Chinese Academy of Sciences, Beijing, and the University of Zaragoza, Spain.

References

Ali, J.R., Thompson, G.M., Song, X., Wang, Y., 2002. Emeishan basalts (SW China) and the "end-Guadalupian" crisis: magnetobiostratigraphic constraints. Journal of the Geological Society 159, 21–29.
An, M., Shi, Y., 2006. Lithospheric thickness of the Chinese continent. Physics of the Earth and Planetary Interiors 159 (3–4), 257–266.
Bai, Z.M., Zhang, Z.J., Wang, Y.H., 2007. Crustal structure across the Dabie–Sulu orogenic belt revealed by seismic velocity profiles. Journal of Geophysics and Engineering 4 (4), 436–442.
Bai, Z.M., Tian, X.B., Tian, Y., 2011. Upper mantle P-wave tomography across the Longmenshan fault belt from passive-source seismic observations along Aba-Longquanshan profile. Journal of Asian Earth Sciences 40 (4), 873–882.
Bassin, C., Laske, G., Masters, G., 2000. The current limits of resolution for surface wave tomography in North America. Eos, Transactions of the American Geophysical Union 81 (48) (Fall Meet Suppl., Abstract S12A-03).
Bielik, M., 1988. A preliminary stripped gravity map of the Pannonian Basin. Physics of the Earth and Planetary Interiors 51 (1–3), 185–189.
Bielik, M., Michael, R., Michael, L., 2013a. Tutorial: the gravity-stripping process as applied to gravity interpretation in the eastern Mediterranean. The Leading Edge 32 (4), 410–416.
Bielik, M., Krajňák, M., Makarenko, I., Legostaeva, O., Starostenko, V.I., Bošanský, M., Grinč, M., Hók, J., 2013b. 3D gravity interpretation of the pre-Tertiary basement in the intramontane depressions of the Western Carpathians: a case study from the Turiec Basin. Geologica Carpathica 64 (5), 399–408.
Braile, L., Chiang, C., 1986. The Continental Mohorovičlć Discontinuity: results from near-vertical and wide-angle seismic reflection studies. Reflection Seismology: A Global Perspective 257–272.
Burov, E., 2010. The equivalent elastic thickness (Te), seismicity and the long-term rheology of continental lithosphere: time to burn-out "crème brûlée"?: insights from large-scale geodynamic modeling. Tectonophysics 484 (1), 4–26.
Cammarano, F., Goes, S., Vacher, P., Giardini, D., 2003. Inferring upper-mantle temperatures from seismic velocities. Physics of the Earth and Planetary Interiors 138 (3), 197–222.
Campbell, I.H., Griffiths, R.W., 1990. Implications of mantle plume structure for the evolution of flood basalts. Earth and Planetary Science Letters 99, 79–93.
Chen, L., Zheng, T.Y., Xu, W.W., 2006. A thinned lithospheric image of the Tanlu Fault Zone, eastern China: constructed from wave equation based receiver function migration. Journal of Geophysical Research 111, B09312.
Chen, C.H., Lee, C.Y., Shinjo, R., 2008. Was there Jurassic paleo-Pacific subduction in South China?: Constraints from $^{40}Ar/^{39}Ar$ dating, elemental and Sr–Nd–Pb isotopic geochemistry of the Mesozoic basalts. Lithos 106 (1), 83–92.
Chen, Y., Zhang, Z.J., Sun, C.Q., Badal, J., 2013. Crustal anisotropy from Moho converted Ps wave splitting analysis and geodynamic implications beneath the eastern margin of Tibet and surrounding regions. Gondwana Research 24 (3–4), 946–957.
Christensen, N.I., Mooney, W.D., 1995. Seismic velocity structure and composition of the continental crust: a global view. Journal of Geophysical Research 100 (B6), 9761–9788.
Chung, S.L., Jahn, B.M., 1995. Plume–lithosphere interaction in generation of the Emeishan flood basalts at the Permian–Triassic boundary. Geology 23, 889–992. http://dx.doi.org/10.1130/0091-7613.
Chung, S.L., Jahn, B.M., Wu, G.Y., Lo, C.H., Cong, B.L., 1998. The Emeishan flood basalt in SW China: a mantle plume initiation model and its connection with continental break-up and mass extinction at the Permian–Triassic boundary. In: Flower, M.F.J., Chung, S.L., Lo, C.H., Lee, T.Y. (Eds.), Mantle Dynamics and Plate Interaction in East Asia. AGU Geodynamic Series, 27, pp. 47–58.
Coffin, M.F., Eldholm, O., 1994. Large igneous provinces: crustal structure, dimensions, and external consequences. Reviews of Geophysics 32, 1–36.
Davis, J.C., 1986. Statistics and Data Analysis in Geology. Wiley, New York.
Deng, Y.F., Li, S.L., Fan, W.M., Liu, J., 2011. Crustal structure beneath South China revealed by deep seismic soundings and its dynamics implications. Chinese Journal of Geophysics 54 (10), 2560–2574 (in Chinese with abstract in English).
Deng, Y., Zhang, Z., Badal, J., Fan, W., 2013. 3-D density structure under South China constrained by seismic velocity and gravity data. Tectonophysics. http://dx.doi.org/10.1016/j.tecto.2013.07.032.
Goes, S., van der Lee, S., 2002. Thermal structure of the North American uppermost mantle inferred from seismic tomography. Journal of Geophysical Research 107 (B3), 2050. http://dx.doi.org/10.1029/2000JB000049.
Goes, S., Spakman, W., Bijwaard, H., 1999. A lower mantle source for central European volcanism. Science 286, 1928–1931.
Goes, S., Govers, R., Vacher, P., 2000. Shallow mantle temperatures under Europe from P and S wave tomography. Journal of Geophysical Research 105 (B5) (11153-11111,11169).
Gradstein, F.M., Ogg, J.G., Schmitz, M.D., 2012. The Geologic Time Scale 2012. Elsevier, Boston, USA. http://dx.doi.org/10.1016/B978-0-444-59425-9.00004-4.
Griffiths, R., Campbell, I., 1991. Interaction of mantle plume heads with the Earth's surface and onset of small-scale convection. Journal of Geophysical Research 96 (B11), 18295–18310.
Hammer, S., 1963. Deep gravity interpretation by stripping. Geophysics 28 (3), 369–378.
He, B., Xu, Y.G., Chung, S.L., Xiao, L., Wang, Y., 2003. Sedimentary evidence for a rapid crustal doming prior to the eruption of the Emeishan flood basalts. Earth and Planetary Science Letters 213, 389–403.
He, B., Xu, Y.G., Wang, Y.M., Luo, Z.Y., 2006. Sedimentation and lithofacies paleogeography in SW China before and after the Emeishan flood volcanism: new insights into surface response to mantle plume activity. Journal of Geology 114, 117–132.
Hu, J.F., Su, Y.J., Zhu, X.G., Chen, Y., 2003. Crustal Vs, Poisson's ratio structures and significances. Science in China Series D: Earth Sciences 33 (8), 714–722 (in Chinese).
Jia, S.X., Li, Z.X., Xu, Z.F., Sheng, F.L., Zhao, W.J., Yang, Z.X., Yang, J., Lei, W., 2006. Crustal structure features of the Leiqiong depression in Hainan Province. Chinese Journal of Geophysics 49 (5), 1385–1394 (in Chinese with abstract in English).
Kaban, M.K., Schwintzer, P., 2001. Oceanic upper mantle structure from experimental scaling of Vs and density at different depths. Geophysical Journal International 147, 199–214.
Larson, R., 1991. Latest pulse of Earth: evidence for a mid-Cretaceous superplume. Geology 19 (6), 547–550.
Laske, G., Masters, G., 1997. A global digital map of sediment thickness. Eos, Transactions of the American Geophysical Union 78, F483.
Lei, J.S., Zhao, D.P., 2006. A new insight into the Hawaiian plume. Earth and Planetary Science Letters 241, 438–453.
Leng, W., Zhong, S., 2010. Surface subsidence caused by mantle plumes and volcanic loading in large igneous provinces. Earth and Planetary Science Letters 291, 207–214.
Li, Z.X., Li, X.H., 2007. Formation of the 1300-km-wide intracontinental orogen and postorogenic magmatic province in Mesozoic South China: a flat-slab subduction model. Geology 35 (2), 179–182.
Li, Y., Oldenburg, D.W., 1996. 3-D inversion of magnetic data. Geophysics 61 (2), 394–408.
Li, Y., Oldenburg, D.W., 1998. 3-D inversion of gravity data. Geophysics 63 (1), 109–119.
Li, G., Zhou, W., 1990. Pictures of Oilfields in China. Petroleum Industry Press, Beijing.
Li, S., Mooney, W., Fan, J., 2006. Crustal structure of mainland China from deep seismic sounding data. Tectonophysics 420 (1–2), 239–252.
Liu, Y.K., Chang, X., 2003. Modeling of burial and subsidence history in Sichuan Basin. Chinese Journal of Geophysics 46 (2), 283–290.
Liu, J., Liu, F., He, J., Chen, H., You, Q., 2001. Study of seismic tomography in Panxi paleorift area of southwestern China—structural features of crust and mantle and their evolution. Science in China (Series D) 44, 277–288.
Liu, C.Z., Liu, Z.C., Wu, F.Y., Chu, Z.Y., 2012. Mesozoic accretion of juvenile subcontinental lithospheric mantle beneath South China and its implications: geochemical and Re–Os isotopic results from Ningyuan mantle xenoliths. Chemical Geology 291, 186–198.
Lo, C.H., Chung, S.L., Lee, T.Y., Wu, G.Y., 2002. Age of the Emeishan flood magmatism and relations to Permian–Triassic boundary events. Earth and Planetary Science Letters 198, 449–458.
Lü, Y., Zhang, Z., Pei, S., Sandvol, E., Xu, T., Liang, X., 2013. 2.5-Dimensional tomography of uppermost mantle beneath Sichuan–Yunnan and surrounding regions. Tectonophysics. http://dx.doi.org/10.1016/j.tecto.2013.03.008.
Luo, Z., Tong, Z., 1988. Plate Tectonics and Sedimentary Basins in China. Publishing House of the Chinese Geoscience University Press, Wuhan.
Montelli, R., Nolet, G., Dahlen, F.A., Masters, G., Engdahl, E.R., Hung, S.H., 2004. Finite-frequency tomography reveals a variety of plumes in the mantle. Science 303 (5656), 338–343.
Montelli, R., Nolet, G., Dahlen, F.A., Masters, G., 2006. A catalogue of deep mantle plumes: new results from finite-frequency tomography. Geochemistry, Geophysics, Geosystems 7, Q11007. http://dx.doi.org/10.1029/2006GC001248.
Mooney, W.D., Kaban, M.K., 2010. The North American upper mantle: density, composition, and evolution. Journal of Geophysical Research 115 (B12), B12424.
Mooney, W., Meissner, R., 1992. Multi-genetic origin of crustal reflectivity: a review of seismic reflection profiling of the continental lower crust and Moho. Continental Lower Crust 23, 45–79.
Mooney, W., Laske, G., Masters, G., 1998. CRUST5.1: a global crustal model at 5° × 5°. Journal of Geophysical Research 103, 727–747.
Morgan, W.B., 1971. Convection plumes in the lower mantle. Nature 230, 42–43.

Nagy, D., 1966. The gravitational attraction of a right rectangular prism. Geophysics 31 (2), 362–371.
Nielsen, C., Thybo, H., 2009. No Moho uplift below the Baikal rift zone: evidence from a seismic refraction profile across southern Lake Baikal. Journal of Geophysical Research 114 (B8), B08306.
Panasyuk, S.V., Hager, B.H., 2000. Models of isostatic and dynamic topography, geoid anomalies, and their uncertainties. Journal of Geophysical Research 105 (B12), 28,199–28,209. http://dx.doi.org/10.1029/2000JB900249.
Pavlis, N.K., Holmes, S.A., Kenyon, S.C., Factor, J.K., 2008. An earth gravitational model to degree 2160: EGM2008. EGU General Assembly, pp. 13–18.
Pavlis, N.K., Holmes, S.A., Kenyon, S.C., Factor, J.K., 2012. The development and evaluation of the Earth Gravitational Model 2008 (EGM2008). Journal of Geophysical Research 117 (B4), B04406.
Prodehl, C., Mooney, W.D., 2012. Exploring the Earth's crust, history and results of controlled-source seismology,. Geological Society of America Memoirs 208, 764.
Ratschbacher, L., Webb, B.R.H.L.E., McWilliams, M., Ireland, T., Dong, S., Calvert, A., Chateigner, D., 2000. Exhumation of the ultrahigh-pressure continental crust. Journal of Geophysical Research 105 (B6), 13,303–313,338.
Rhodes, M., Davies, J.H., 2001. Tomographic imaging of multiple mantle plumes in the uppermost lower mantle. Geophysical Journal International 147, 88–92.
Ritsema, J., Allen, R.M., 2003. The elusive mantle plume. Earth and Planetary Science Letters 207, 1–12.
Rohm, A.H.E., Snieder, R., Goes, S., Trampert, J., 2000. Thermal structure of continental upper mantle inferred from S-wave velocity and surface heat flow. Earth and Planetary Science Letters 181, 395–407.
Romanowicz, B., Gung, Y., 2002. Superplumes from the core–mantle boundary to the lithosphere: implications for heat flux. Science 296, 513–516.
Serón, F.J., Badal, J.I., Sabadell, F.J., 2001. Spatial prediction procedures for regionalization and 3-D imaging of Earth structures. Physics of the Earth and Planetary Interiors 123, 149–168.
Shapiro, N.M., Ritzwoller, M.H., 2004. Thermodynamic constraints on seismic inversions. Geophysical Journal International 157, 1175–1188.
Shellnutt, J.G., 2013. The Emeishan large igneous province: a synthesis. Geoscience Frontiers. http://dx.doi.org/10.1016/j.gsf.2013.07.003.
Shellnutt, J.G., Denyszyn, S.W., Mundil, R., 2012. Precise age determination of mafic and felsic intrusive rocks from the Permian Emeishan large igneous province (SW China). Gondwana Research 22, 118–126.
Sun, C.Q., Lei, J.S., Li, C., Zhang, G.W., Zha, X.H., Li, F., 2013. Crustal anisotropy beneath the Yunnan region and dynamic implications. Chinese Journal of Geophysics 56 (12), 4095–4105 (in Chinese with abstract in English).
Teng, J., Zhang, Z., Zhang, X., Wang, C., Gao, R., Yang, B., Qiao, Y., Deng, Y., 2013. Investigation of the Moho discontinuity beneath the Chinese mainland using deep seismic sounding profiles. Tectonophysics. http://dx.doi.org/10.1016/j.tecto.2012.11.024.
Tian, X., Teng, J., Zhang, H., Zhang, Z., Zhang, Y., Yang, H., Zhang, K., 2011. Structure of crust and upper mantle beneath the Ordos Block and the Yinshan Mountains revealed by receiver function analysis. Physics of the Earth and Planetary Interiors 184 (3), 186–193.
Wang, Q.C., 2009. Preliminary discussion on sedimentary tectonics of the clustered continents of South China. Acta Sedimentologica Sinica 27 (5), 811–817 (in Chinese with abstract in English).
Wang, C., Zhang, X., Chen, B., Chen, X., Song, S., Zheng, J., Hu, H., Lou, H., 1997. Crustal structure of Dabieshan orogenic belt. Science in China (Series D) 40 (5), 456–462.
Wang, C., Chan, W., Mooney, W.D., 2003. Three-dimensional velocity structure of crust and upper mantle in southwestern China and its tectonic implications. Journal of Geophysical Research 108. http://dx.doi.org/10.1029/2002JB001973.
Wang, Q.S., An, Y.L., Zhang, C.J., Jiang, F.Z., 2003. Gravitology. Seismological Press, Beijing.
Wang, C.Y., Wu, J.P., Lou, H., Zhou, M.D., Bai, Z.M., 2003. P-wave crustal velocity structure in western Sichuan and eastern Tibetan region. Science in China (Series D) 46 (Suppl. II), 254–265.
Wang, Q., Xu, J.F., Jian, P., Bao, Z.W., Zhao, Z.H., Li, C.F., Xiong, X.L., Ma, J.L., 2006. Petrogenesis of adakitic porphyries in an extensional tectonic setting, Dexing, South China: implications for the genesis of porphyry copper mineralization. Journal of Petrology 47 (1), 119.
Wang, Q.S., Tang, D.Z., Peng, M.X., Du, B., 2010. Well logging response features and identification of non-sandstone reservoirs in Jianghan Basin. Journal of Oil and Gas Technology 32 (2), 73–77 (in Chinese).
Wedepohl, K.H., 1995. The composition of the continental crust. Geochimica et Cosmochimica Acta 59 (7), 1217–1232.
White, R.S., McKenzie, D.P., 1989. Magmatism at rift zones: the generation of volcanic continental margins and flood basalts. Journal of Geophysical Research 94, 7685–7729.
Wignall, P., Sun, Y., Bond, D.P.G., Izon, G., Newton, R.J., Védrine, S., Widdowson, M., Ali, J.R., Lai, X., Jiang, H., 2009. Volcanism, mass extinction, and carbon isotope fluctuations in the Middle Permian of China. Science 324, 1179–1182. http://dx.doi.org/10.1126/science.1171956.
Wu, J., Zhang, Z., 2012. Spatial distribution of seismic layer, crustal thickness, and Vp/Vs ratio in the Permian Emeishan Mantle Plume region. Gondwana Research 22 (1), 127–139.
Xiong, S.B., Zheng, Y., Yin, Z.X., Zeng, X.X., Quan, Y.L., Sun, K.Z., 1993. The 2-D structure and its tectonic implications of the crust in the Lijiang–Panzhihua–Zhehai region. Chinese Journal of Geophysics (Acta Geophysica Sinica) 36 (4), 434–444 (in Chinese with abstract in English).
Xiong, X., Gao, S., Li, Q.S., Lu, Z.W., Wang, H.Y., Li, W.H., Guan, Y., 2009. The Moho depth of South China revealed by seismic probing. Acta Geoscientica Sinica 30 (6), 774–786 (in Chinese with abstract in English).
Xu, Y.G., He, B., 2007. Thick and high velocity crust in Emeishan large igneous province, SW China: evidence for crustal growth by magmatic underplating/intraplating. In: Foulger, G., Jurdy, D. (Eds.), The Origins of Melting Anomalies: Plates, Plumes, and Planetary Processes. Geological Society of America Special Publication, 430, pp. 841–858.
Xu, Y.G., Chung, S.L., Jahn, B.M., Wu, G.Y., 2001. Petrologic and geochemical constraints on the petrogenesis of Permian–Triassic Emeishan flood basalts in southwestern China. Lithos 58, 145–168.
Xu, Y.G., He, B., Chung, S., Menzies, M.A., Frey, F.A., 2004. Geologic, geochemical, and geophysical consequences of plume involvement in the Emeishan flood-basalt province. Geology 32 (10), 917–920.
Xu, Y.G., He, B., Huan, X.L., Luo, Z.Y., Chung, S.L., Xiao, L., Zhu, D., Shao, H., Fan, W.M., Xu, J.F., Wang, Y.J., 2007. Identification of mantle plumes in the Emeishan Large Igneous Province. Episodes 30, 32–42.
Yao, B.H., Zhang, Z.Q., Wang, J.L., Huo, E.J., Zhang, X.K., Liu, B.J., Wu, J.S., Wang, F.Y., Yu, P., Mao, Y.P., 2007. Prospecting and research on fine crustal structure by using multi-geophysics survey methods in Shanghai region. Chinese Journal of Geophysics 50 (2), 482–491 (in Chinese with abstract in English).
Zeng, H.L., 2005. Gravity Field and Gravity Exploration. Geological Publishing House, Beijing 79–100.
Zhang, Y., Chen, H., Lu, K., 1996. Tectonic framework and formation of sedimentary basins in China. Science in China (Series D) 26, 493–498.
Zhang, Z., Mahoney, J.J., Mao, J., Wang, F., 2006. Geochemistry of picritic and associated basalt flows of the western Emeishan flood basalt province, China. Journal of Petrology 47 (10), 1997–2019.
Zhang, Z.J., Wang, Y.H., Chen, Y., Houseman, G.A., Tian, X.B., Wang, E.Q., Teng, J.W., 2009. Crustal structure across Longmenshan fault belt from passive source seismic profiling. Geophysical Research Letters 36, L17310. http://dx.doi.org/10.1029/2009GL039580.
Zhang, Z., Yuan, X., Chen, Y., Tian, X., Kind, R., Li, X., Teng, J., 2010. Seismic signature of the collision between the east Tibetan escape flow and the Sichuan Basin. Earth and Planetary Science Letters 292 (3–4), 254–264.
Zhang, Z., Yang, L., Teng, J., Badal, J., 2011. An overview of the earth crust under China. Earth-Science Reviews 104 (1–3), 143–166. http://dx.doi.org/10.1016/j.earscirev.2010.10.003.
Zhang, Z.J., Deng, Y.F., Teng, J.W., Wang, C.Y., Gao, R., Chen, Y., Fan, W., 2011. An overview of the crustal structure of the Tibetan plateau after 35 years of deep seismic soundings. Journal of Asian Earth Sciences 40, 977–989. http://dx.doi.org/10.1016/j.jseaes.2010.03.010.
Zhao, D., 2001. Seismic structure and origin of hotspots and mantle plumes. Earth and Planetary Science Letters 192, 251–265.
Zhao, D., 2007. Seismic images under 60 hotspots: search for mantle plumes. Gondwana Research 12, 335–355.
Zhong, S., Watts, A.B., 2002. Constraints on the dynamics of mantle plumes from uplift of the Hawaiian Islands. Earth and Planetary Science Letters 203, 105–116.
Zhong, Y.T., He, B., Mundil, R., Xu, Y.G., 2014. CA-TIMS zircon dating of felsic ignimbrite from the uppermost lava succession in the Emeishan Large Igneous Province. Lithos (submitted for publication).
Zhu, J.F., Xu, X.W., Zhang, X.K., 2005. Inspection and research on fine crust construction by using deep seismic reflection, high-resolution seismic refraction and seismic wide angle reflection/refraction. Science in China (Series D) 35 (8), 738–749 (in Chinese).
Zhu, J.S., Cai, X.L., Cao, J.M., Yan, Z.Q., 2006. Lithospheric structure and geodynamics in China and its adjacent areas. Geology in China 33 (4), 793–803 (in Chinese with abstract in English).